# CHAPTER IV

# RESULTS AND DISCUSSION

## Part A: The actinomycete *Micromonospora* sp. BTG 10-2

Twenty two actinomycetes selected from different sources of soils in Thailand were tested for the antimicrobial activity by agar disc diffusion method against pathogenic bacteria and yeast. The result of the antimicrobial activity tested screening was shown in Table 4.1. The locations of the collection sources are listed below.

- Mountain soil, Ratchaburi
- Mangrove soil, Krabi
- Peat swamp soil, Kanchanaburi
- Peat swamp soil, Trang
- Peat swamp soil, Phatthalung
- Peat swamp soil, Yala
- Peat swamp soil, Narathiwat

*Micromonospora* sp. BTG 10-2 isolated from peat swamp soil at Baan Toong Kong in Narathiwat province showed the best antimicrobial activity against gram positive bacteria including *M. luteus* ATCC 9341 and *B. subtilis* ATCC 6633 with clear zones of 35 and 29 mm and against gram negative bacteria, *Ps. aeruginosa* ATCC 27853, *E. coli* ATCC 25922 and *Salmonella* sp. with clear zones of 16, 9 and 8 mm at concentration 1 mg/disc, respectively; however, it showed no activity against *C. albicans* ATCC 10231.

**Table 4.1** The antimicrobial activity screening test by agar disc diffusion method

| Code name | Diameter of the inhibitory zones (mm) against | | | | | |
|---|---|---|---|---|---|---|
| | *M. luteus* | *B. subtilis* | *E.coli* | *Ps. aeruginosa* | *Salmonella* sp. | *C. albicans* |
| 1-1 | 9 | N/C | N/C | N/C | 6.5 | N/C |
| 1-2-3 | 8 | 17 | N/C | N/C | N/C | N/C |
| 11-9-11 | 14 | 8 | N/C | N/C | 6.5 | N/C |
| 13-28 | 17 | 6.5 | 6.5 | N/C | 9 | N/C |
| 13-41 | 10 | N/C | 6.5 | N/C | 8 | N/C |
| 13-54 | 20 | 19 | N/C | N/C | N/C | N/C |
| 7-1-1 | 9 | 7 | 6.5 | N/C | N/C | N/C |
| 7-2-2 | 12 | 6.5 | 6.5 | N/C | 9 | N/C |
| BTG1-13 | 27 | 15 | N/C | N/C | 10 | N/C |
| BTG3-3 | 8 | 7 | N/C | N/C | 6.5 | N/C |
| BTG6-1 | 6.5 | N/C | N/C | N/C | 8 | N/C |
| BTG7-3 | 22 | 12 | N/C | N/C | 9 | N/C |
| BTG7-5 | N/C | N/C | N/C | N/C | 8 | N/C |
| BTG10-2 | 35 | 29 | 9 | 16 | 8 | N/C |
| KK2-6 | 7 | 7 | N/C | N/C | N/C | N/C |
| LK7-1 | 27 | 14 | 7 | 10 | 10 | N/C |
| LK2-4 | 25 | 13 | N/C | N/C | 6.5 | N/C |
| TJ2-2 | N/C | N/C | N/C | N/C | N/C | N/C |
| YK2-1 | 10 | N/C | N/C | N/C | 7.5 | N/C |
| TK2-5 | 19 | 9 | N/C | N/C | 8 | N/C |
| TT2-10 | 9 | 6.5 | 6.5 | N/C | N/C | N/C |
| Unidentify | 20 | 13 | N/C | N/C | N/C | N/C |

* N/C = no clear zone

## 1. Characteristics of *Micromonospora* sp. BTG 10-2

The actinomycete strain BTG10-2 was isolated from a soil sample collected from a peat swamp forest (pH 4.29) at Baan Toong Kong in Narathiwat Province, Thailand. This strain exhibited a range of phenotypic and chemotaxonomic properties that are consistent with the genus *Micromonospora* (Kawamoto, 1989). They produced well-developed and branched substrate hyphae on yeast extract-malt extract medium, but no aerial hyphae. Spores were borne singly on the substrate hyphae having approximately diameter of 0.5-0.6 μm. The spores were smooth on the surface and non-motile. The color of the substrate mycelium was vivid orange. Then the dark brown to black spores was formed later within and at the surface of the colonies which darken as a result of sporulation. The scanning electron micrograph and the colonial appearance of *Micromonospora* sp. BTG 10-2 were shown in Figures 4.1, 4.2, and 4.3.

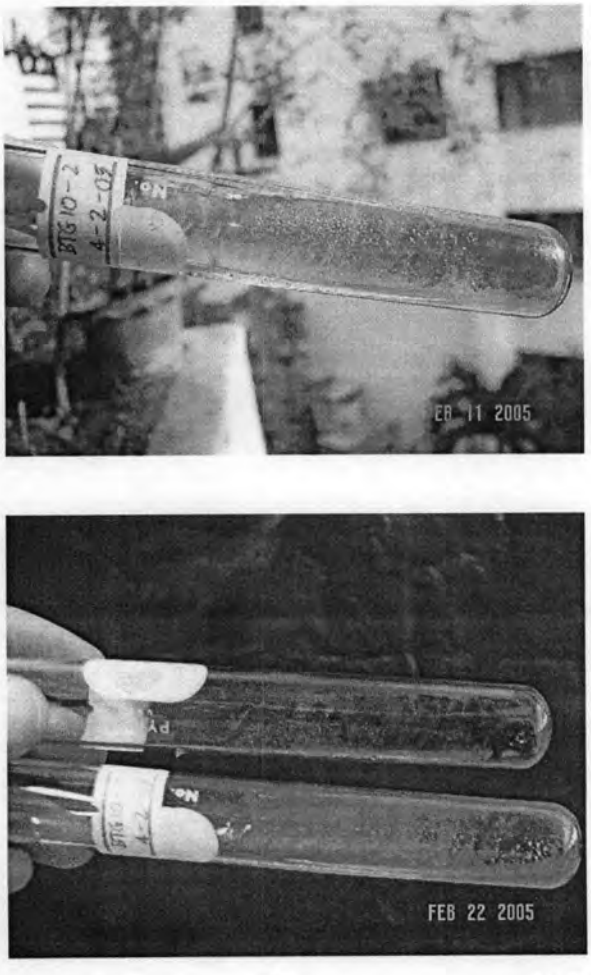


(a)

(b)

**Figure 4.1** The colonial appearance of *Micromonospora* sp. BTG 10-2 on YM slants at 7 days (a) and 18 days (b)

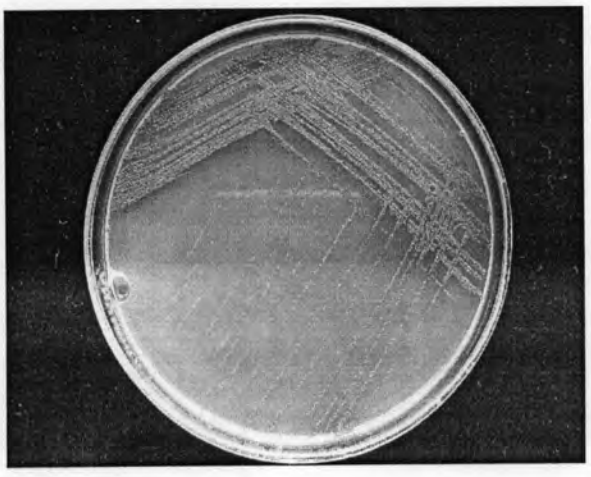

**Figure 4.2** The colonial appearances of *Micromonospora* sp. BTG 10-2 on the YMA medium (21 days)

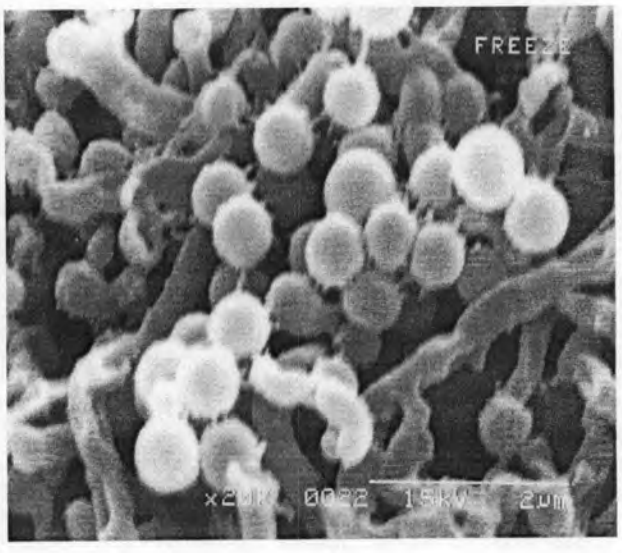

**Figure 4.3** The scanning electron micrograph of *Micromonospora* sp. BTG 10-2 on YMA medium (21 days)

## 2. Fractionation of the ethyl acetate extract

*Micromonospora* sp. BTG 10-2 was cultivated in yeast extract–malt extract medium (YM broth) totally 17.5 L. The fermentation broth was extracted with ethyl acetate to yield 1.5 g of ethyl acetate extract. The ethyl acetate extract was further separated by chromatographic methods to give fraction M41332, 2.5 mg (0.16% yielded based on the ethyl acetate extract) as shown in Scheme 4.1. Due to the limited amount and the decomposition of M41332, the fraction was partially characterized for the constituents by analyses of its NMR spectral data. The proton and carbons

assignment of M41332 was established by analyses of DEPT 135, DEPT 90, $^{1}H - {}^{1}H$ COSY and HMQC NMR spectra and comparison with literature data of known anthracycline derivatives. (Ahmed *et al.*, 2005; Kim *et al.*, 2000; Mackay *et al.*, 1996; Parkinson *et al.* 1995)

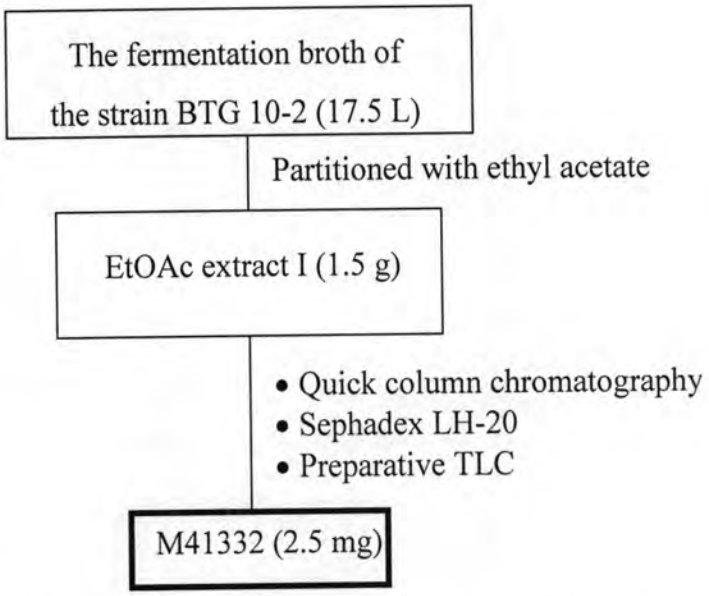


**Scheme 4.1** Fractionation of **M41332** from *Micromonospora* sp. BTG 10-2

### 3. Characterization of M41332

Compound M41332 was obtained as a yellow-brown oily liquid. The UV spectrum in $CH_2Cl_2$ of M41332 exhibited $\lambda_{max}$ at 259 nm and 427 nm. The 300 MHz $^{1}H$-NMR spectrum of M41332 in $CDCl_3$ (Figure 4.4) revealed that it contained three methyl proton signals at δ 0.85, 1.13, and 2.39 ppm; five methylene proton signals at δ 1.23, 2.24, 2.39, 2.56, and 4.01 ppm; and nine methine proton signals at δ 3.96, 4.12, 4.54, 4.71, 5.46, 7.33, 7.69, 7.84, and 7.86 ppm. The 75 MHz $^{13}C$-NMR spectrum of compound M41332 in $CDCl_3$ (Figure 4.5) gave twenty-five carbon signals. The carbon signals were classified by the DEPT 135 spectrum, DEPT 90 spectrum (Figure 4.5) and HMQC spectrum as three methyl carbon signals at δ 14.77, 24.24, and 28.03 ppm; five methylene carbons at δ 22.72, 30.09, 32.21, 36.10, and 55.40 ppm; nine methine carbons at δ 44.39, 63.95, 70.12, 78.72, 97.14, 119.80, 121.14, 125.73, and 137.28 ppm; and eight quaternary carbons at δ 210.53, 188.40, 187.65, 163.33, 159.78, 143.38, 133.48, and 116.41 ppm.

Analyses of the $^1H - ^1H$ COSY and HMQC spectra in $CDCl_3$ established six partial structures including fragments **a, b, c, d, e**, and **f**. The aromatic region in the $^1H$-NMR spectrum showed the presence of three consecutive aromatic protons as an ABC system at δ 7.84 (1H, d, $J$ = 7.7 Hz, H-1), 7.69 (1H, dd, $J$ = 7.7, 8.3 Hz, H-2) and 7.33 ppm (1H, d, $J$ = 8.3 Hz, H-3), suggestive of the trisubstituted benzene ring. The singlet proton at δ 7.86 ppm (1H, s, H-9) also suggested the second aromatic ring. In addition, the carbonyl carbon at δ 187.6 ppm (C-10) showed HMBC correlations to protons at δ 7.84 (H-1) and 7.86 (H-9) ppm (Figure 4.6(a)); the oxygenated carbon (C-4) at δ 163.33 ppm to H-2 at δ 7.69 ppm; C-1 (δ 119.98 ppm) to H-3 (δ 7.83 ppm); C-4a (δ 116.4 ppm) to H-1 (δ 7.89 ppm); C-10a (δ 133.5 ppm) to H-2 (δ 7.69 ppm); and C-5a (δ 115.3 ppm) to H-9 (δ 7.86 ppm). These NMR data supported the nature of the anthraquinone nucleus of Fragment **a**.

The presence of an acetyl group ($\delta_H$ = 2.39, $\delta_C$ = 28.22 ppm) was confirmed by the HMBC correlation to carbonyl signal at δ 210.58 ppm (Fragment **b**) (Figure 4.6(b)). There was $^1H$–$^1H$ COSY correlations from the methine proton at δ 4.71 ppm (1H, br q, $J$ = 6.3 Hz) to methyl proton at δ 1.13 ppm (3H, d, $J$ = 6.3 Hz) (Fragment **c**) (Figure 4.6(c)). Fracment **d** was identified by the $^1H$–$^1H$ COSY correlations from two methylene protons at δ 4.0 ppm ($\delta_C$ = 54 ppm) and δ 2.7 ppm ($\delta_C$ = 36 ppm) which correlated with another methine proton at δ 5.1 ppm (Figure 4.6(d)). There was also $^1H$–$^1H$ COSY correlations from the methine proton at δ 4.2 ppm (br s, $\delta_C$ = 44.4 ppm) to methylene proton at δ 2.3 and 2.6 ppm (Fragment **e**) (Figure 4.6(e)). The anomeric proton (1H, d, $J$ = 3.3 Hz) which resonated downfield in the region δ 5.46 ppm was identified in the $^1H$–$^1H$ COSY spectrum due to its correlations to the metylene protons at δ 1.73 and 2.42 ppm, which correlated with another methine proton at δ 3.69 ppm (br s, $\delta_C$ = 70 ppm) (Fragment **f**) (Figure 4.6(f)).

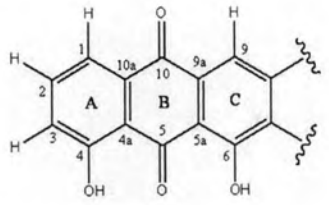


Fragment a

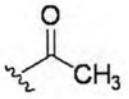


Fragment b

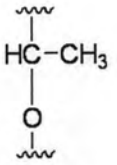


Fragment c

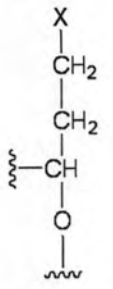


Fragment d

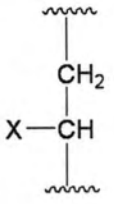


Fragment e

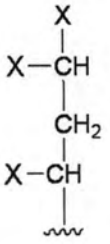


Fragment f

However, the author could not finish the structure elucidation because this partially purified fraction was unstable and the yield was too small to continue the processes. The crude ethyl acetate extract from *Micromonospora* sp. BTG10-2 exhibited very interesting results of antimicrobial activities against the pathogenic bacteria. The compound isolated from the *Micromonospora* sp. BTG10-2 had low stability, being very sensitive to acid condition.

## Part B: The endophytic fungus *Exseroholum rostratum* RNAS5

### 1. Identification and characterization of the strain RNAS5

The endophytic fungus strain RNAS5 was isolated from a surface-sterilized leaf of *Rhinacanthus nasutus* (ทองพันชั่ง). The fungus was identified based on the microscopic morphology and the analysis of DNA sequences of the ITS region of ribosomal RNA gene. The results indicated that endophytic fungus RNAS5 is *Exserohilum rostratum* (Drechsler) (Leonard and Suggs, 1974). The appearance was a black broth with a black mycelia spreading over the surface area (Figure 4.7).

### 2. Extraction and purification of the ethyl acetate extract of *Exserohilum rostratum* RNAS5

After 21 days of incubation at 25°C, the SDB fermentation broth (total 20 L) of RNAS5 was separated from mycelia by filtering through 4 layers of cotton gauze and partitioned with ethyl acetate to yield 2.9 g of the red ethyl acetate extract and 391.2 mg of the white precepitate. The white precipitate was fractionated by normal phase flash column chromatography, using gradient MeOH in $CH_2Cl_2$ as the solvents. Compound **W3** (21.7 mg) was obtained as a white powder. The red crude ethyl acetate extract was separated on a silica gel column. Gradient elution with EtOAc, hexane, $CH_2Cl_2$, and MeOH mixtures was used, and two compounds (compounds **R5-9** and **R4/2-7**) were obtained. Compound **R5-9** was identified as the known compound, rostratin A (total 61.3 mg, 2.11% yield of the red ethyl acetate extract) were obtained as light yellow crystals. Compound **R4/2-7** (34.2 mg, 1.18% yield of the ethyl acetate extract) was obtained as a white powder. The chemical structures of these compounds were determined by analyses of spectroscopic data, including IR, UV, NMR, Mass spectra, and x-ray crystallography as well as by comparison with the literature data.

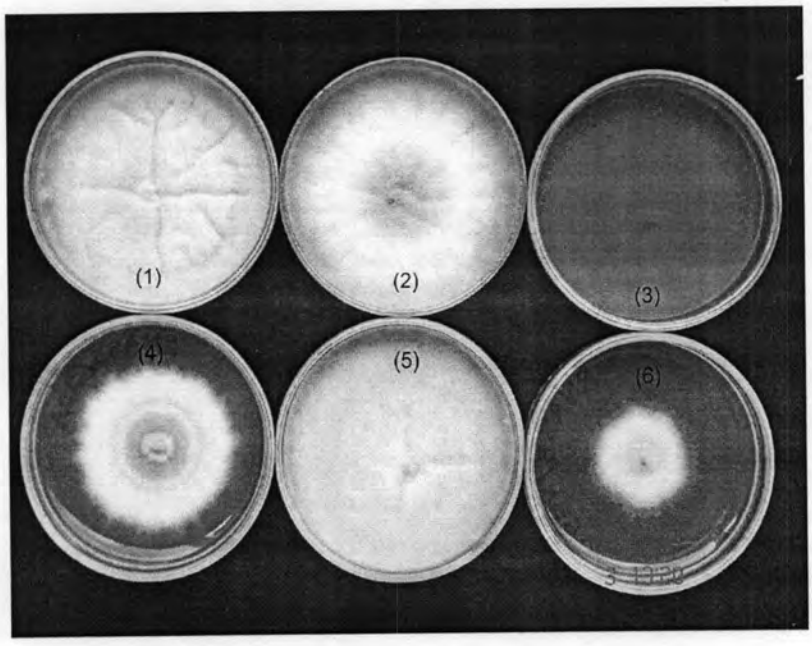


(a)

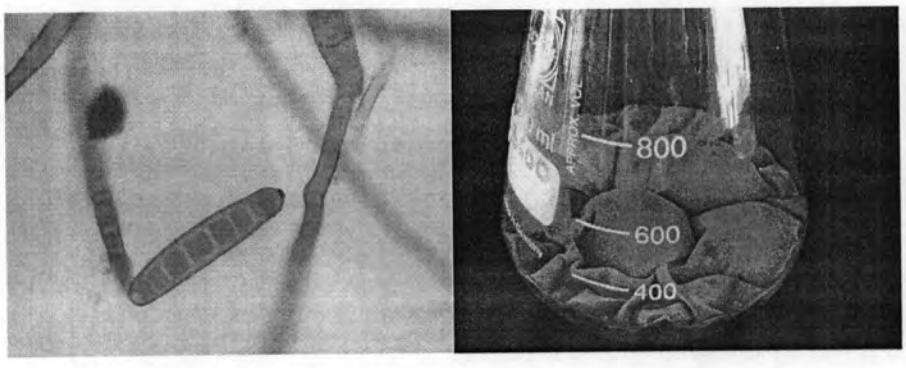


(b) (c)

**Figure 4.7** Morphological characteristic of the endophytic fungus *Exserohilum rostratum* RNAS5

(a) The colonial appearance in difference media:

(1) Malt Czapek agar (MCzA),

(2) Malt extract agar (MEA),

(3) Potato dextrose agar (PDA),

(4) Sabouraud's dextrose agar (SDA),

(5) Yeast Czapek agar (YCzA)

(6) Yeast extract sucrose agar (YES)

(b) Conidia observed under a microscope (x 400)

(c) The appearance of the SD fermentation broth at 21 days

## 3. Structure elucidation of the isolated compounds

### 3.1 Compound R5-9 (rostratin A)

The low-resolution EI mass spectrum of compound **R5-9** showed the molecular ion at *m/z* 428. The HREI mass spectrum showed a fragment ion at *m/z* 364.1652 ($C_{18}H_{24}N_2O_6$) produced through elimination of $S_2$ from the molecular ion of **R5-9**. These combined mass spectral data allowed the molecular formula of **R5-9** to be assigned as $C_{18}H_{24}N_2O_6S_2$ (Figure 4.8). The UV spectrum of **R5-9** (Figure 4.9) displayed maximum absorption at 207.2 nm.

The 500 MHz $^1$H-NMR spectrum of compound **R5-9** in pyridine-$d_6$ (Figure 4.10), used as the NMR solvent, showed twelve proton signals; six methylene proton signals at δ 1.52, 1.63, 2.14, 2.22, 2.98, and 3.02 ppm; four methine proton signals at δ 2.57, 3.45, 3.83, and 3.92 ppm; and two hydroxyl protons at δ 4.94 and 6.71 ppm (Table 4.1). The 125 MHz $^{13}$C-NMR spectrum in pyridine-$d_6$ (Figure 4.11) showed nine carbon signals which are classified by DEPT 135 (Figure 4.12) as three methylene carbon signals at δ 30.55, 32.70, and 33.58 ppm; four methine carbon signals at δ 48.02, 68.80, 69.80, and 70.50 ppm; and two quarternary carbon signals at δ 75.66 and 164.74 ppm (Table 4.1).

Analysis of the $^1$H-$^1$H COSY (Figures 4.13, 4.14) spectrum of **R5-9** recorded in pyridine-$d_6$ established the connectivity from $H_2$-3 (δ 2.98, 1H, dd, $J$ = 5.9, 13.8 Hz and δ 3.02, 1H, t, $J$ = 13.8 Hz) to H-4 (δ 2.57, 1H, ddd, $J$ = 4.5, 5.9, 11.5 Hz); H-4 to H-5 (δ 3.83, 1H, dt, $J$ = 4.5, 10.1 Hz) and H-9 (δ 3.45, 1H, dd, $J$ = 9.3, 11.5 Hz); H-5 to 5-OH (δ 4.94, 1H, s) and $H_2$-6 (δ 1.63, 1H, ddd, $J$ = 3.7, 4.0, 13.1 Hz and δ 2.14, 1H, ddd, $J$ = 3.9, 4.5, 13.1 Hz); and $H_2$-7 (δ 1.52, 1H, ddd, $J$ = 3.7, 4.5, 13.6 Hz and δ 2.22, 1H, dd, $J$ = 3.9, 13.6 Hz) to H-8 (δ 3.92, 1H, dt, $J$ = 4.5, 9.3 Hz) as shown in Figure 4.15.

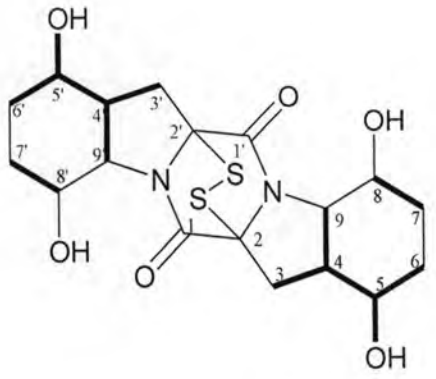


**Figure 4.15** The correlations (bold line) in the $^{1}H$-$^{1}H$ COSY spectrum of compound **R5-9**

The carbon complete assignments of **R5-9** were obtained from the HMBC spectrum (Figures 4.17 and 4.18) showing the following long-range correlations; the quaternary carbons at δ 164.74 (C-1) and 75.66 (C-2) correlated with the methylene protons at δ 2.98 ($H_a$-3) and δ 3.02 ($H_b$-3), both of which showed additional correlations with methine carbon signal at δ 48.02 (C-4), 68.80 (C-5), and 70.5 (C-9). Furthermore, both the C-4 and C-9 carbon signals yielded HMBC correlations to H-5 (δ 3.83) and H-8 (δ 3.92) protons, which also correlated with the two methylene carbons at δ 32.70 (C-6) and δ 30.55 (C-7). The long-range correlations from the HMBC spectrum of **R5-9** in pyridine-$d_6$ are shown in Figure 4.19 and summarized in Table 4.1.

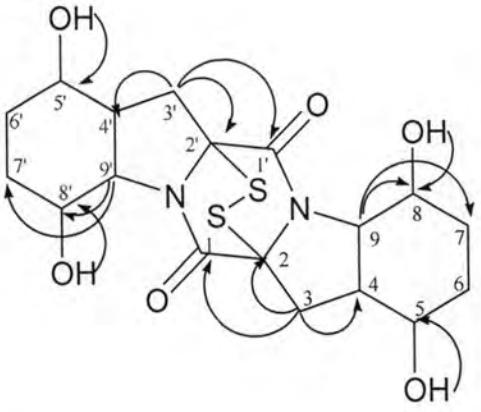


**Figure 4.19** The $^{1}H$-$^{13}C$ long-range correlations in the HMBC spectrum of compound **R5-9** in pyridine-$d_6$

These $^{1}H$ and $^{13}C$ NMR data accounted for only half of the carbon and hydrogen composition given by the molecular formula. This observation demonstrated that **1** was a highly symmetrical structure compound. These overall data defined a phenylalanine-

derived diketopiperazine dimmer. Consistent with the literature data, the disulfide bridge in **R5-9** was positioned between carbons C-2 and C-2'.

The ring juncture protons H-4/4' and H-9/9' both showed a large vicinal coupling constant (11.5 Hz) consistent with a *trans*-diaxial ring juncture. Using this as a starting point, the remaining relative stereochemistry of **R5-9** was established using NOESY spectral data (Figure 4.20). From NOESY data, H-9/9' showed NOE correlations with the $H_a$-3/3', H-5/5', and $H_a$-7/7', demonstrating that these three protons were spatially arranged on the bottom face of the molecule (all axial protons). As expected, NOE correlations were not observed between H-9/9' and H-4/4'; instead, H-4/4' showed a clear NOE correlation with H-8/8', indicating these protons were in axial positions on the top face of the molecule. Since H-5/5' and H-8/8' had both been defined as axial, the hydroxyl groups at these carbons were assigned equatorial positions.

Comparison of the spectral data of **R5-9** to those reported in the literature (Tan *et al.*, 2004) confirmed that it is the highly symmetrical diketopiperazine, rostratin A. Rostratin A was isolated from the whole broth of the marine-derived fungus *Exserohilum rostratum* (Drechsler), a fungus strain found associated with a marine cyanobacterial mat.

Next, the author determined the absolute stereochemistry of **R5-9** by X-ray crystallography. The compound was crystallized from ethyl acetate as a white crystal. Compound **R5-9** crystallized in the monoclinic space group C2 with $a$ = 16.561 (3), $b$ = 8.6374 (17), $c$ = 7.5245 (15) Å, and $\beta$ = 109.20 (3)° with one molecule of composition $C_{18}H_{24}N_2O_6S_2$ forming the symmetric unit. The final crystallographic discrepancy index was 0.0335 for the observed reflections. The x-ray crystal structure in *ORTEP* representation and molecular packing are shown in Figures 4.21 and 4.22. The absolute configurations of R5-9 could be assigned from the x-ray crystallographic data as 2/2'*R*, 4/4'*S*, 5/5'*S*, 8/8'*S*, 9/9'*S* which were in agreement with the literature. The absolute configuration of rostratin A was previously determine by the Mosher's method (Tan *et al.*, 2004).

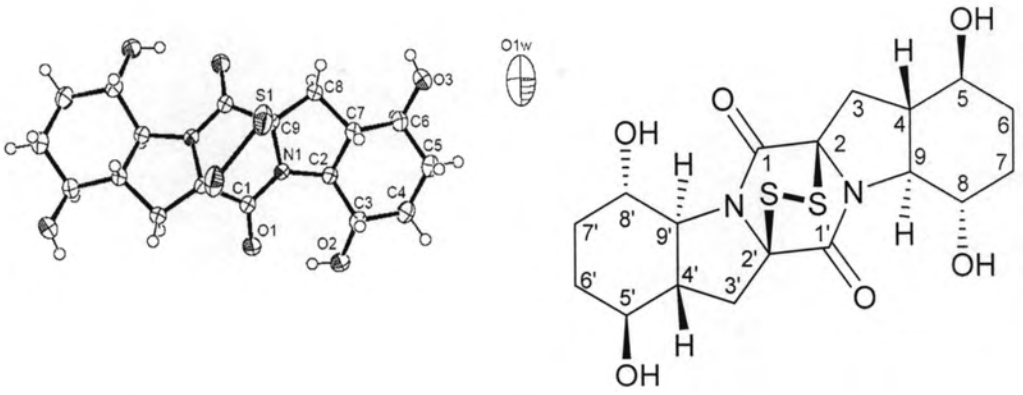


**Figure 4.21** X-ray crystal structure of compound **R5-9**: *ORTEP* representation

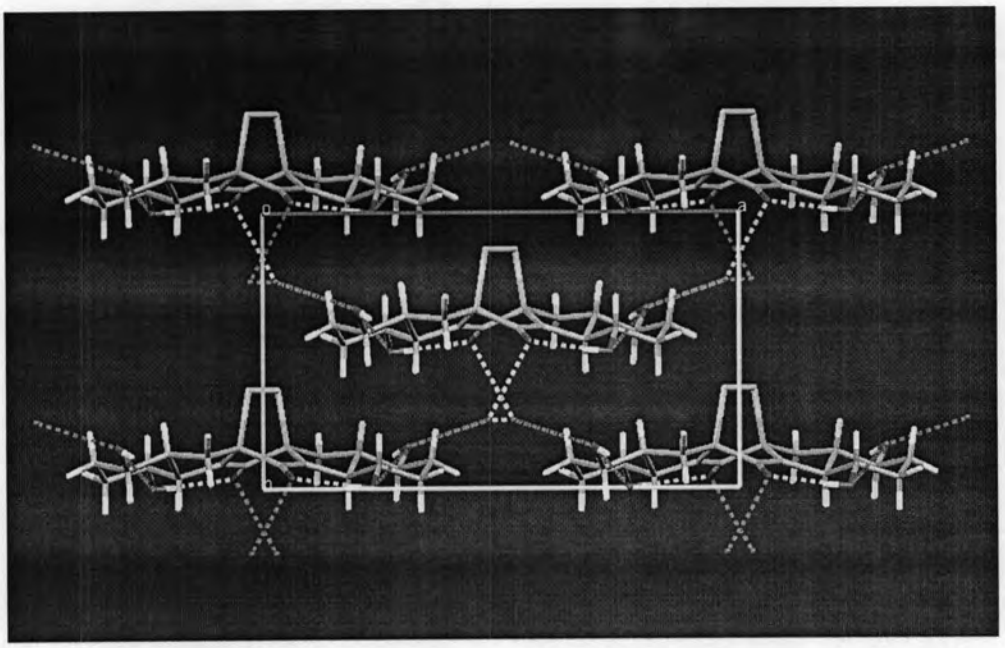

**Figure 4.22** X-ray crystal structure of compound **R5-9**: Molecular packing

**Table 4.2:** NMR spectral assignments for compound **R5-9** in pyridine – $d_6$

| Position | $\delta_C$ | $\delta_H$ (multi., *J* in Hz) | $^1H$-$^1H$ COSY | HMBC correlation $^{13}C$ to $^1H$ |
|---|---|---|---|---|
| 1/1' | 164.74 | | | 3/3' |
| 2/2' | 75.66 | | | 3/3' |
| 3/3' | 33.58, $CH_2$ | (a) 2.98 (dd, 13.8, 5.9) | 3/3'(b), 4/4' | 4/4' |
| | | (b) 3.02 (t, 13.8) | 3/3'(a), 4/4' | |
| 4/4' | 48.02, CH | 2.57 (ddd, 4.5, 5.9, 11.5) | 3/3'(ab), 5/5', 9/9' | 3/3', 6/6', 9/9' |
| 5/5' | 68.80, CH | 3.83 (dt, 10.1, 4.5) | 4/4', 5/5'-OH, 6/6' | 3/3', 5/5'-OH, 6/6' |
| 6/6' | 32.70, CH | (a) 1.63 (ddd, 3.7, 4.0, 13.1) | 5/5', 6/6'(b) | 4/4', 8/8'-OH |
| | | (b) 2.14 (ddd, 3.9, 4.5, 13.1) | 5/5', 6/6'(a) | |
| 7/7' | 30.55, $CH_2$ | (a) 1.52 (ddd, 3.7, 4.5, 13.6) | 8/8' | 8/8', 9/9' |
| | | (b) 2.22 (dd, 3.9, 13.6) | | |
| 8/8' | 69.80, CH | 3.92 (dt, 9.3, 4.5) | 7/7' | 7/7', 8/8'-OH, 9/9' |
| 9/9' | 70.50, CH | 3.45 (dd, 11.5, 9.3) | 4/4' | 3/3', 5/5' |
| 5/5'-OH | | 4.94 (s) | 5/5' | |
| 8/8'-OH | | 6.71 (s) | | |

**Table 4.3:** NMR spectral assignments for compound **R5-9** as compared with rostratin A in DMSO – $d_6$

| Position | Compound R5-9 | | Rostratin A | |
|---|---|---|---|---|
| | $\delta_C$ | $\delta_H$ (multi., *J* in Hz) | $\delta_C$ | $\delta_H$ (multi., *J* in Hz) |
| 1/1' | 164.99 | | 164.7 | |
| 2/2' | 75.96 | | 75.9 | |
| 3/3' | 33.92, $CH_2$ | (a) 2.40 (dd, 14.19, 5.34) | 33.9, $CH_2$ | (a) 2.41 (dd, 14.4, 5.2) |
| | | (b) 2.58 (t, 13.55) | | (b) 2.59 (dd, 14.4, 12.2) |
| 4/4' | 48.33, CH | 2.06 (dq, 11.90, 5.49) | 48.3, CH | 2.09 (dddd, 12.2, 12.0, 11.7, 5.2) |
| 5/5' | 69.10, CH | 3.51 (dt, 9.77, 4.88) | 69, CH | 3.52 (dddd, 11.7, 10.7, 5.2, 4.8) |
| 6/6' | 33.05, $CH_2$ | (a) 1.24 (m) | 33.1, $CH_2$ | (a) 1.30 (m) |
| | | (b) 1.85 (m) | | (b) 1.85 (m) |
| 7/7' | 30.91, $CH_2$ | (a) 1.31 (m) | 31.0, $CH_2$ | (a) 1.26 (m) |
| | | (b) 1.94 (m) | | (b) 1.95 (m) |
| 8/8' | 70.02, CH | 3.62 (dt, 9.16, 4.27) | 70.0, CH | 3.64 (ddd, 12.5, 10.5, 5.8) |
| 9/9' | 70.77, CH | 3.38 (dd, 11.59, 9.16) | 70.7, CH | 3.41 (dd, 12.0, 10.5) |
| 5/5'-OH | | 5.06 (d, 5.2) | | 5.08 (d, 4.8) |
| 8/8'-OH | | 6.06 (s) | | 6.08 (s) |

### 3.2 Compound W3 (exserohilin A)

Compound **W3** was obtained as a white powder. The HREI mass spectrum of **W3** showed a molecular ion at *m/z* 422.0637, allowing the molecular formula of **W3** to be assigned as $C_{18}H_{18}N_2O_6S_2$ (Figure 4.23). The IR absorption spectrum (Figure 4.24) displayed characteristic bands at 3,354 $cm^{-1}$ (hydroxyl stretching) and 1,682 $cm^{-1}$ (C=O stretching). The UV spectrum of **W3** in MeOH (Figure 4.25) displayed maximum absorption at 207.2 nm.

The 500 MHz $^1$H-NMR spectrum of **W3** in pyridine-$d_6$ (Figure 4.26, 4.26(a) and 4.26(b)) showed nine proton signals; four methylene proton signals at δ 3.11/3.21, and 3.32/3.48 ppm; four methine proton signals at δ 3.40, 3.87, 4.78, and 5.23 ppm; and one hydroxyl protons at δ 8.48 ppm (Table 4.3). The 125 MHz $^{13}$C-NMR spectrum in pyridine-$d_6$ (Figure 4.27) showed nine carbon signals which were classified by DEPT 135 (Figure 4.28) as two methylene carbon signals at δ 42.55 and 44.76 ppm; four methine carbon signals at δ 42.83, 46.41, 61.98, and 66.05 ppm; and a quarternary carbon signal at δ 72.21; the amide carbonyl signal at δ 160.46, and the ketone carbonyl signal at δ 207.23 ppm (Table 4.3).

Analysis of the $^1$H-$^1$H COSY (Figure 4.29) spectrum of **W3** recorded in pyridine-$d_6$ established the correlations of $H_2$-3 to H-4 (δ 3.40, 1H, dd, $J$ = 9.0, 12.3 Hz), and H-4 to H-9 (δ 5.23, 1H, dd, $J$ = 2.8, 9.0 Hz); $H_2$-6 to H-7 (δ 3.87, 1H, dd, $J$ = 4.4, 6.7 Hz), and H-7 to H-8 (δ 4.78, 1H, dd, $J$ = 2.8, 4.4 Hz) and the partial structures are shown in Figure 4.30.

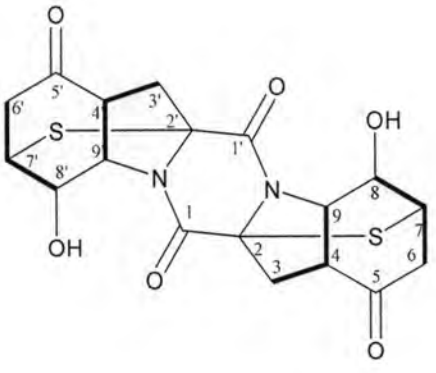


**Figure 4.30** The correlations (bold line) in the $^1$H-$^1$H COSY spectrum of compound **W3**

These $^{1}H$ and $^{13}C$ NMR data accounted for only half of the carbon and hydrogen compositions given by the molecular formula. This observation demonstrated that **W3** was also a highly symmetrical structure compound.

The proton-carbon complete assignments of **W3** were obtained from the HMBC spectra (Figures 4.32 and 4.33) showing the following long-range correlations; the two carbonyl carbon signals at δ 160.46 (C-1/1') correlated with the methylene protons at δ 3.11 (1H, dd, $J$ = 12.3, 13.7 Hz, $H_a$ -3/3') and at δ 207.23 (C-5/5') correlated with the methylene protons at δ 3.11 ($H_a$ -3/3'), 3.21 (1H, d, $J$ = 13.7 Hz, $H_b$ -3/3'), 3.40 (H-4/4'), 3.32 (1H, d, $J$ = 18.9 Hz, $H_a$ -6/6'), 3.48 (1H, dd, $J$ = 6.7, 18.9 Hz, $H_b$ -6/6'), and 3.87 (H-7/7') ppm. The assignment of the quaternary carbon signal at δ 72.23 ppm (C-2/2') was supported by the HMBC correlations to H-3/3', H-4/4'. Additional HMBC correlation of C-2/2' to H-7/7' (δ 3.87) assured the placement of the sulfide bridges between C-2/2' and C-7/7'. HMBC correlations of C-4/4' (δ 46.41) to $H_{ab}$ -3/3' (δ 3.11 and 3.21), and H-8/8' (δ 4.78); the C-7/7' (δ 42.83) showed correlations to H-9/9' (δ 5.23); C-8/8' (δ 66.05) to H-4/4' (δ 3.40), $H_b$ -6/6' (δ 3.48), and H-9/9' (δ 5.23); and C-9/9' (δ 61.98) to 8/8'-OH (δ 8.48) completed the connectivity of the fragments. The long-range correlations from the HMBC spectrum of **W3** in pyridine-$d_6$ were shown in Figure 4.34 and summarized in Table 4.3.

**Table 4.4** NMR spectral assignments for compound **W3** in pyridine – $d_6$

| Position | $\delta_C$ | $\delta_H$ (mmultipli., $J$ in Hz) | $^{1}H$-$^{1}H$ COSY | HMBC correlation $^{13}C$ to $^{1}H$ |
|---|---|---|---|---|
| 1/1' | 160.46 | | | 3/3' |
| 2/2' | 72.21 | | | 3/3', 4/4', 7/7', 9/9' |
| 3/3' | 44.76, $CH_2$ | (a) 3.11 (dd, 13.7, 12.3) | | 4/4', 9/9' |
| | | (b) 3.21 (d, 13.7) | | |
| 4/4' | 46.41, CH | 3.40 (dd, 9.0, 12.3) | $3/3'_a$ | 3/3', 8/8' |
| 5/5' | 207.23 | | | 3/3', 4/4', 6/6', 7/7' |
| 6/6' | 42.55, CH | (a) 3.32 (d, 18.9) | | 3/3', 8/8' |
| | | (b) 3.48 (dd, 18.9, 6.7) | | |
| 7/7' | 42.83, CH | 3.87 (dd, 4.4, 6.7) | $6/6'_b$, 8/8' | 6/6', 8/8'-OH, 9/9' |
| 8/8' | 66.05, CH | 4.78 (dd, 2.8, 4.4) | 7/7' | 4/4', 6/6', 9/9' |
| 9/9' | 61.98, CH | 5.23 (dd, 2.8, 9.0) | 4/4' | $3/3'_b$, 4/4', 8/8'-OH |
| 8/8'-OH | | 8.48 (br s) | | |

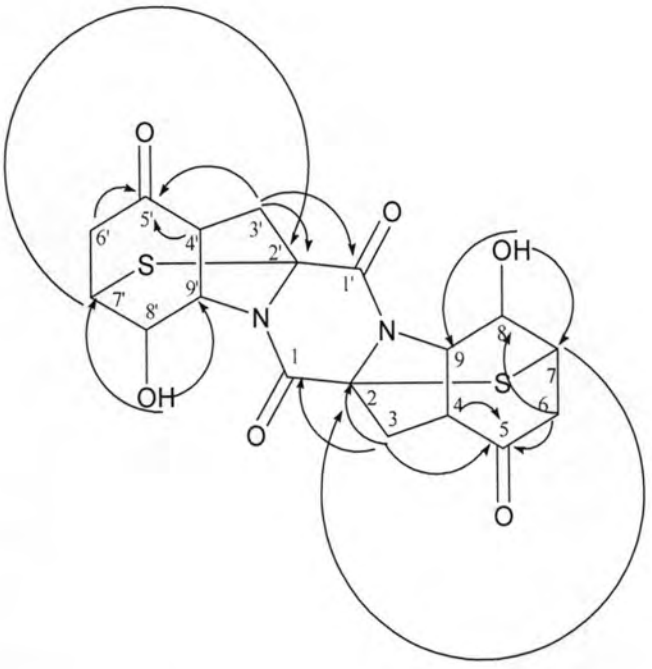


**Figure 4.34** The important $^{1}H$-$^{13}C$ long-range correlations in the HMBC spectrum of compound **W3** in pyridine-$d_6$

The ring juncture protons H-4/4' and H-9/9' both showed a large vicinal coupling constant (9.0 Hz) consistent with a *cis*-ring juncture. Using this as a starting point, the remaining relative stereochemistry of **W3** was established using NOESY spectral data (Figure 4.35). As expected, H-4/4' showed clear NOESY correlations with H-9/9' and H-7/7' confirming these protons were in the same face of the molecule. The sulfide bridges between C-2/2' and C-7/7' forced the cyclohexanone ring existed in boat conformation. Therefore, the NOESY correlations of H-9/9' to H-8/8' and H-8/8' to H-7/7' could not be used to assigned the configuration at C-8/8'. However, the multiplicities among these protons are identical to those of compound **R4/2-7**. The relative configuration at C-8/8' were assigned based on this information. These observed NOESY confirmed the relative configurations of **W3** as shown the complete structure in Figure 4.36.

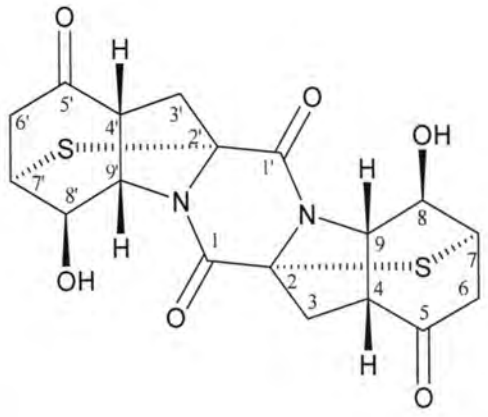

**Figure 4.36** The structure of compound **W3**

By analyses of these available spectral data and comparison of the NMR spectral data of **W3** with of those rostratin series that were reported in the literature (Tan *et al.*, 2004), compound **W3** was identified as a new highly symmetrical diketopiperazine compound, and named as a new series exserohilin A.

### 3.3 Compound R4/2-7 (exserohilin B)

Compound **R4/2-7** was obtained as a white powder. The HREI mass spectrum of compound **R4/2-7** showed a molecular ion at *m/z* 454.0307, allowing the molecular formula of **R4/2-7** to be assigned as $C_{18}H_{18}N_2O_6S_3$ (Figure 4.37). The UV spectrum of **R4/2-7** (Figure 4.38) displayed maximum absorption at 207.2 nm.

The 500 MHz $^1$H-NMR spectrum of compound **R4/2-7** in pyridine-$d_6$ (Figure 4.39), as the solvent, showed eighteen proton signals; four pair of methylene proton signals at δ 2.89/3.59, 2.98/3.34, 3.05/3.18, and 3.31/3.43 ppm; eight methine proton signals at δ 3.39, 3.48, 3.87, 3.92, 4.78, 5.05, 5.21 and 5.37 ppm; and two hydroxyl protons at δ 8.25 and 8.45 ppm. The multiplicity and coupling constants are listed in Table 4.4. The 125 MHz $^{13}$C-NMR spectrum in pyridine-$d_6$ (Figure 4.40) showed eighteen carbon signals which are classified by DEPT 135 (Figure 4.41) as four methylene carbon signals at δ 38.86, 42.33, 44.62, and 46.61 ppm; eight methine carbon signals at δ 43.43, 44.65, 46.31, 47.20, 61.86, 63.88, 65.51, and 65.81 ppm; and six quarternary carbon signals at δ 71.51, 75.27, 161.53, 161.13, 207.28, and 207.63 ppm (Table 4.4).

Analysis of the $^1$H-$^1$H COSY (Figure 4.42) spectrum of compound **R4/2-7** recorded in pyridine-$d_6$ established the first partial structure from H-3 to H-4 (δ 3.48,

1H, dd, $J$ = 8.3, 8.6 Hz); H-4 to H-9 (δ 5.05, 1H, dt, $J$ = 4.1, 8.6 Hz); H-9 to H-8 (δ 5.37, 1H, dd, $J$ = 3.1, 4.1 Hz); H-8 to H-7 (δ 3.87, 1H, dd, $J$ = 4.6, 5.9 Hz); and H-7 to $H_b$-6 (δ 3.59, 1H, dd, $J$ = 5.9, 19.2 Hz). And the second partial structure from H-12 to H-13 (δ 3.39, 1H, dd, $J$ = 8.9, 12.2 Hz); H-13 to H-18 (δ 5.21, 1H, dt, $J$ = 2.2, 8.9 Hz); H-18 to H-17 (δ 4.78, 1H, dt, $J$ = 2.2, 4.5 Hz); H-17 to H-16 (δ 3.92, 1H, dd, $J$ = 2.2, 6.1 Hz); and H-16 to $H_b$-15 (δ 3.43, 1H, dd, $J$ = 6.1, 18.5 Hz) shown summarized in Figure 4.43.

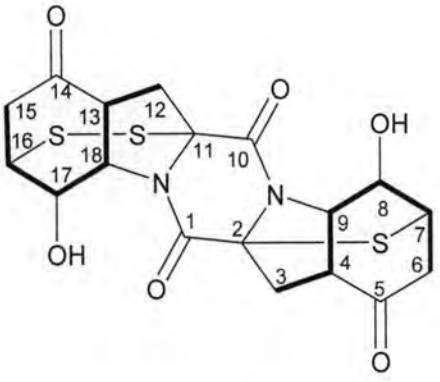


**Figure 4.43** The correlations (bold line) in the $^1$H-$^1$H COSY spectrum of compound **R4/2-7**

The complete $^{13}$C assignments of compound **R4/2-7** were obtained from the HMBC spectra (Figures 4.45 and 4.46) showing the following long-range correlations; the two carbonyl carbon signals at δ 163.13 (C-1) and 161.53 (C-10) correlated with the methylene protons at δ 3.05 (1H, dd, $J$ = 12.2, 13.7 Hz, $H_a$-3) and 2.98 (1H, dd, $J$ = 8.3, 13.2 Hz, $H_a$-12) ppm, respectively. Another two carbonyl carbon signals at δ 207.28 (C-5) correlated with the methylene protons at δ 3.05 ($H_a$-3), 3.18 (1H, d, $J$ = 12.2 Hz, $H_b$-3), 3.31 (1H, d, $J$ = 18.5 Hz, $H_a$-6), 3.43 ($H_b$-6), and the methine proton at δ 3.92 (H-7) ppm, and at δ 207.63 (C-14) correlated with the methylene protons at δ 2.98 ($H_a$-12), 3.34 (1H, d, $J$ = 13.2 Hz, $H_b$-12), 2.89 (1H, d, $J$ = 19.2 Hz, $H_a$-15), 3.59 ($H_b$-12), and the methine protons at δ 3.48 (H-13), and 5.05 (H-18) ppm. The assignment of the quaternary carbon signal at δ 75.27 ppm (C-11) was supported by the HMBC correlations to H-12, H-13, and H-18. The other quaternary carbon signal at δ 71.51 ppm (C-2) was supported by HMBC correlations to H-3, H-4 (δ 3.39), and H-9 (δ 5.21). Additional HMBC correlation of C-2 to H-7 (δ 3.87) assured the placement of the sulfide bridge between C-2 and C-7. There was no HMBC correlation from C-11 to H-16, so we put the disulfide bond from C-11 to C-16. By comparison with compound

**W3**, the chemical shift of C-2 (δ 71.51) of **R4/2-7**, which contain the sulfide bridge, was closer to that of C-2/2' (δ 72.33) of **W3** than C-11 (δ 75.25) of **R4/2-7**. The long-range correlations from the HMBC spectrum of compound **R4/2-7** in pyridine-$d_6$ were shown in Figure 4.47 and summarized in Table 4.4.

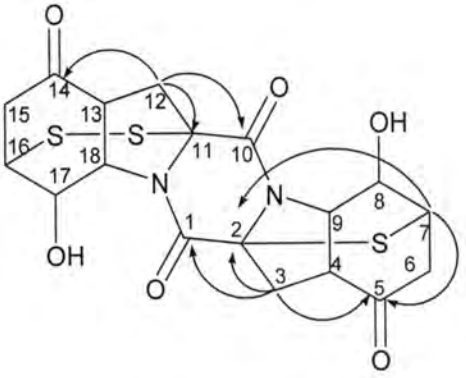


**Figure 4.47** The important $^{1}H$-$^{13}C$ long-range correlations in the HMBC spectrum of compound **R4/2-7** in pyridine-$d_6$

The ring juncture protons H-4/H-9 and H-13/H-18 both showed the large vicinal coupling constants, 8.9 and 8.6 Hz, respectively, consistent with a *cis*-ring junctures. Using these as a starting point, the remaining relative stereochemistry of **R4/2-7** was established using NOESY spectral data (Figure 4.48). As expected, H-4 showed a clear NOESY correlation with H-9 and H-7, as same as H-13 showed a clear NOESY correlation with H-18 and H-16 confirming these protons were on the same face of the molecule. The sulfide bridge between C-2 and C-7, as well as the disulfide bridge between C-11 and C-16, forced the cyclohexanone ring existed in boat conformation. Therefore, the NOESY correlations of H-9 to H-8 and H-8 to H-7, as well as the NOESY correlations of H-18 to H-17 and H-17 to H-16, could not be used to assigned the configuration at C-8 and C-17. However, the absolute configurations at C-8 and C-17 were assigned based on the x-ray crystallographic information as show the complete structure in Figure 4.49.

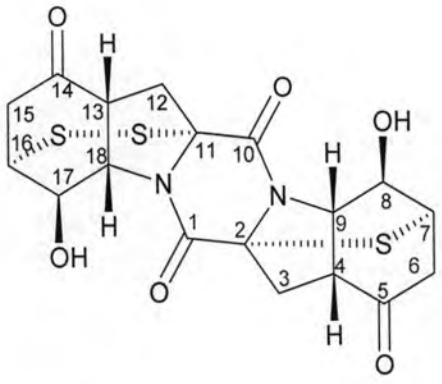

**Figure 4.49** The structure of compound **R4/2-7**

We determined the absolute stereochemistry of **R4/2-7** by X-ray crystallography. The compound was obtained as the colorless crystals from DMSO. Compound **R4/2-7** crystallized in the orthorhombic space group $P2_12_12_1$ with $a$ = 7.52490 (10), $b$ = 11.0832 (2), 22.7007 (4) Å, with one molecule of composition $C_{18}H_{18}N_2O_6S_3$ forming the asymmetric unit. The final crystallographic discrepancy index was 0.0298 for the observed reflections. The x-ray crystal structure in *ORTEP* representation and molecular packing are shown in Figures 4.50 and 4.51. And the absolute configuration of **R4/2-7** is 2*R*, 4*R*, 7*R*, 8*R*, 9*S*, 11*R*, 13*R*, 16*R*, 17*R*, 18*S*.

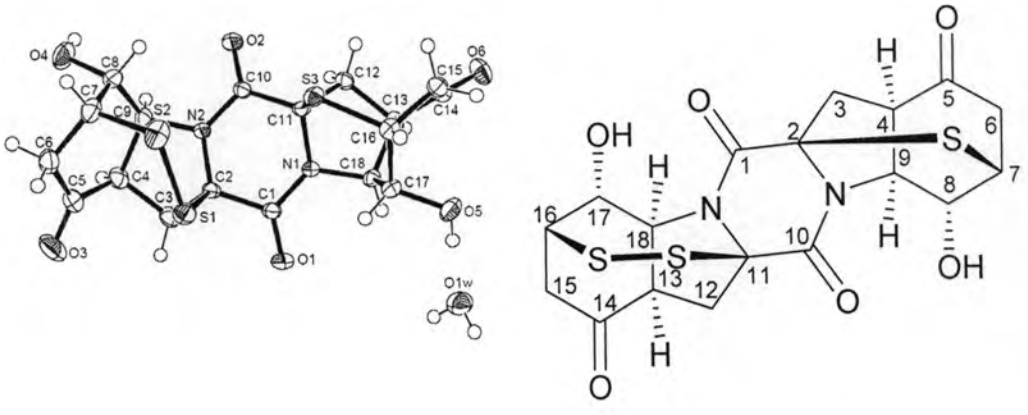

**Figure 4.50** X-ray crystal structure of compound **R4/2-7**: *ORTEP* representation

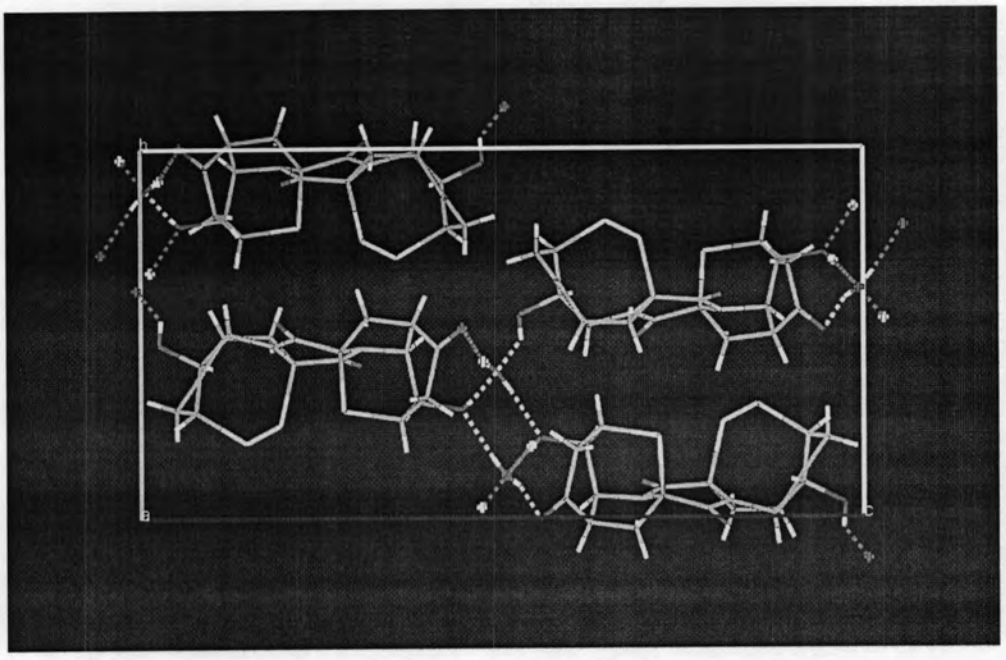

**Figure 4.51** X-ray crystal structure of compound **R4/2-7**: Molecular packing

By analyses of these available spectral data and comparison of the NMR spectral data of **R4/2-7** with of those rostratin series that reported in the literature (Tan *et al.*, 2004) and compound **W3**, compound **R4/2-7** was identified as a new diketopiperazine compound, but it was a non-symmetric compound, and named as a new series exserohilin B.

**Table 4.5** NMR spectral assignments for compound **R4/2-7** in pyridine – $d_6$

| Position | $\delta_C$ | $\delta_H$ (multi., *J* in Hz) | $^1H$-$^1H$ COSY | HMBC correlation $^{13}C$ to $^1H$ |
|---|---|---|---|---|
| 1 | 163.13, C | | | 12a |
| 2 | 71.51, C | | | 12ab,13,16,18 |
| 3 | 44.62, $CH_2$ | (a) 3.05(dd, 12.2, 13.7) | | 13,15a,18 |
| | | (b) 3.18(d, 13.7) | | |
| 4 | 46.31, CH | 3.39 (dd, 8.9, 12.2) | 12ab | 12a,17 |
| 5 | 207.28, C | | | 12ab,15ab,16 |
| 6 | 42.33, $CH_2$ | (a) 3.31(d, 18.5) | | 12b |
| | | (b) 3.43(dd, 6.1, 18.5) | | |
| 7 | 43.43, CH | 3.92 (dd, 6.1, 2.2) | 15b | 15a,18 |
| 8 | 65.51, CH | 4.78 (br s) | 16 | 15b,18 |
| 8 – OH | | 6.18 (d, 2.8) | | 16,17,18 |
| 9 | 61.86, CH | 5.21 (br d, 8.9) | 13,16 | 12b |
| 10 | 161.53, C | | | 3a |
| 11 | 75.27, C | | | 3ab,4,9 |
| 12 | 46.61, $CH_2$ | (a) 2.98 (dd, 8.3, 13.2) | | 4 |
| | | (b) 3.34 (d, 13.2) | | |
| 13 | 44.68, CH | 3.48 (dd, 8.3, 8.6) | 3ab | 3ab,8,9 |
| 14 | 207.63, C | | | 3ab,4,6ab,9 |
| 15 | 38.86, $CH_2$ | (a) 2.89 (d, 19.2) | | 3a,8 |
| | | (b) 3.59 (dd, 5.9, 19.2) | | |
| 16 | 47.20, CH | 3.87 (br s) | 6b | 6ab,9 |
| 17 | 65.81, CH | 5.37 (dd, 3.1, 4.1) | 7,9 | 3b,6a,9 |
| 17–OH | | 6.06 (d, 4) | | 7,8,9 |
| 18 | 63.88, CH | 5.05 (br d, 8.6) | 4 | 3b |

**4. Biological activities**

From the determination of antibacterial activities by broth microdilution method, test bacteria used in this study were *Staphylococcus aureus* ATCC 25923, *Bacillus subtilis* ATCC 6633, *Escherichia coli* ATCC 25922 and *Pseudomonas aeruginosa* ATCC 27853. The compounds R5-9, W3, and R4/2-7 were tested at the final concentration of 64 μg/ml. The experiment was done in duplicate. After incubation at 37 °C for 24 hours, a 20-μl of *p*-iodonitrotetrazolium (INT) solution (1 mg/ml) was added into each well. The assay plates were further incubated for 1 hour. Violet color developed in each well indicated the growth of tested organism. The well that showed no change in color indicated antibacterial activity of the test compound.

Anti- *C. albicans* activity of R5-9, W3, and R4/2-7 was determined by broth microdilution method. The compounds were tested at the final concentration of 64 μg/ml. The experiment was done in duplicate. After incubation at 37 °C for 24 hours, a 20-μl of *p*-iodonitrotetrazolium (INT) solution (1mg/ml) was added into each well. The assay plates were further incubated for 24 hours. Violet color developed in each well indicated the growth of test organism. The well that showed no change in color indicated anti- *C. albicans* activity of the test compound.

The crude EtOAc extract of endophytic fungus, *Exserohilum rostratum* RNAS5 showed synergistic activity with ketoconazole against *C. albicans*. But it was found that R5-9, W3, and R4/2-7 had no activity against test microorganisms.